Dalton Transactions

Accepted Manuscript

ROYAL SOCIETY OF CHEMISTRY

www.rsc.org/dalton

Methanolysis of Ammonia Borane by Shape-Controlled Mesoporous Copper Nanostructures for Hydrogen Generation

Qilu Yao,[a#] Ming Huang,[b#] Zhang-Hui Lu,[a*] Yuwen Yang,[a] Yuxin Zhang,[b*] Xiangshu Chen,[a*] Zhen Yang[a]

[a]*Jiangxi Inorganic Membrane Materials Engineering Research Centre, College of Chemistry and Chemical Engineering, Jiangxi Normal University, Nanchang, 330022, China;* [b]*College of Materials Science and Engineering, Chongqing University, Chongqing 400044, China*

Diverse mesoporous CuO nanostructures have been prepared by a facile and scaleable wet-chemical method and reduced to mesoporous Cu nanostructures by using the reductant of ammonia borane (AB). These mesoporous Cu nanostructures have been applied as catalyst for hydrogen generation from the methanolysis of AB. The catalytic results show that the reaction rate and the amount of hydrogen evolution significantly relied on their morphologies. Compared with the nanosheets-like, bundle-like and dandelion-like Cu, the flower-like Cu nanostructures exhibit the highest catalytic activity with total turnover frequency (TOF) value of 2.41 mol H_2 mol catalyst^{-1} min^{-1} and a low activation energy value of 34.2 ± 1.2 kJ mol^{-1} at room temperature. Furthermore, the flower-like Cu nanostructures has also shown an excellent activity in recycle tests. The low cost and high performance of Cu nanocatalysts may have high potential to find its practical application in hydrogen generation from the methanolysis of AB.

[#]These authors contributed equally to this work.

*E-mail: luzh@jxnu.edu.cn (Z.–H. Lu), zhangyuxin@cqu.edu.cn (Y.X. Zhang), cxs66cn@jxnu.edu.cn (X.S. Chen).

1. Introduction

Nowadays, hydrogen is considered to be one of the most promising energy carriers in the future owing to its clean burning nature, environmental friendliness, and high energy content. The search for safe and efficient hydrogen storage materials remains one of the most difficult challenges on the way to a hydrogen-powered society as a long-term solution to solve energy problems.[1-6] Due to the high hydrogen capacity and environmentally friendly nature, ammonia borane (AB) complex is recognized as one of the most promising candidates for chemical hydrogen storage.[7-14] In general, the release of hydrogen from AB can be obtained through thermal dehydrogenation in solid state, and solvolysis (hydrolysis and methanolysis) in solution.[15-18] Among these dehydrogenation routes, solvolysis process appears to be more practical for applications because of high temperature and power consumption requirement of the thermolysis of AB. Only in the presence of suitable catalysts, dehydrogenation of AB in solvolysis can be achieved under ambient atmosphere at room temperature.[19-34] Catalytic hydrolysis of ammonia borane has been well studied by various transition metal catalysts.[7,8,11,12] Nevertheless, small quantities of ammonia can be liberated from hydrolytic dehydrogenation from AB at high concentrations.[16,35-40] This can pose problems in practical applications. Yet, using methanol instead of water could overcome this difficult problem.[16] The present catalytic methanolysis reaction can be

briefly expressed as follows:

$$NH_3BH_3 + 4CH_3OH \rightarrow NH_4B(OCH_3)_4 + 3H_2 \quad (1)$$

More importantly, the methanolysis product of $NH_4B(OCH_3)_4$ can be converted back to AB by reaction with $LiAlH_4$ in the presence of NH_4Cl.

So far various catalysts such as $RuCl_3$, $RhCl_3$, $PdCl_2$, $CuCl_2$, $NiCl_2$, Raney-Ni,[16] PVP-stabilized Pd NPs,[35] PVP-stabilized Ru NPs,[36] zeolite stabilized Rh NPs,[37] Ru immobilized in MMT,[38] $Co_{48}Pd_{52}/C$,[39] Co-Co_2B, Ni-Ni_3B, and Co-Ni-B[40] have been studied for hydrogen generation from the methanolysis of AB, among which the Ru species have been regarded as one of the most activity ones.[16,35-40] However, the high cost of Ru catalysts hindered its wide rang of application. Therefore, great efforts have been made to search for first-row metal based catalysts.

In this work, mesoporous CuO nanostructures with diverse morphologies have been prepared via a facile and scaleable wet-chemical method. The obtained different shapes of mesoporous CuO were firstly reduced to mesoporous Cu by AB under ambient condition, and then used as a robust and cost-effective catalyst in hydrogen generation from the methanolysis of AB. The flower-like mesoporous Cu nanostructures catalyst shows the highest catalytic activity with a total turnover frequency (TOF) of 2.41 mol H_2 mol catalyst^{-1} min^{-1}, in comparison to the nanosheets-like, bundle-like and dandelion-like Cu, for hydrogen generation from the methanolysis of AB. The effect of catalysts concentration, reaction temperatures and recyclability of catalysts have also been investigated and discussed, respectively.

2. Experimental section

2.1. Chemicals

Copper nitrate ($Cu(NO_3)_2 \cdot 3H_2O$), ethanol (C_2H_5OH), sodium hydrate (NaOH), ammonia ($NH_3 \cdot H_2O$), tetraoctylammonium bromide (TOAB), methanol (CH_3OH), and solvents used in this work were purchased from Alfa Aesar. Ammonia borane (NH_3BH_3, AB, 90%) was purchased from Aldrich. The entire chemicals were of analytical purity and used without any further purification.

2.2. Synthesis of mesoporous Cu with diverse shapes

Mesoporous CuO nanostructures with diverse shapes were prepared via a facile and scaleable wet-chemical method.[41,42] The detailed experimental process could be found in the supplementary data. The mesoporous Cu with diverse shapes were then obtained as the catalysts by reducing the as-prepared mesoporous CuO with diverse shapes. In a typical experiment, the as-synthesized mesoporous CuO (0.15 mmol) were dispersed in 5.0 mL methanol. The reduction reaction initiated when 34.3 mg AB was added into the flask with vigorous shaking, resulting in the generation of mesoporous Cu nanocatalyst, which was used as catalyst for hydrogen generation from the methanolysis of AB.

2.3. Methanolysis of AB catalyzed by mesoporous Cu with diverse shapes

Catalytic reactions were carried at room temperature using a two-necked round-bottomed flask with one of the flask openings connected to a gas buret and another used for the introduction of ammonia borane. 5.0 mL methanol suspension of 0.15 mmol of mesoporous Cu (synthesized as described above) was kept in the reaction flask. The catalytic methanolysis of AB for the release of hydrogen was

started by adding 34.3 mg AB into the flask with vigorous shaking. The reaction was completed when there was no more gas generation.

2.4. Recyclability of mesoporous Cu with diverse shapes in the methanolysis of AB

For the recyclability test of catalysts, after the hydrogen generation reaction was completed, further equivalent of NH_3BH_3 (34.3 mg, 90%) was subsequently added to the reaction flask 20 min later and the released gas was monitored by the gas burette. The reactions were repeated for five times under ambient atmosphere at room temperature. After cycle test, the catalysts were separated from the reaction solution by centrifugation, washed with water for three times and dried in vacuum oven at 313 K overnight.

2.5. Characterization

Powder X-ray diffraction (XRD) studies were performed on a Rigaku RINT-2200 X-ray diffractometer with a $Cu_{K\alpha}$ source (40 kV, 20 mA). The morphologies and sizes of the CuO nanostructures were carried out with high-resolution transmission electron microscopy (HRTEM, ZEISS LIBRA 200), field emission scanning electron microscopy (FESEM, FEI NOVA 400) and focused ion beam (ZEISS AURIGA FIB/SEM). The Surface area measurements were performed by N_2 adsorption at liquid nitrogen temperature using automatic volumetric adsorption equipment (Belsorp mini II). Temperature programmed desorption (TPD) experiments were measured on a Micromeritics AutoChem II 2920 system, and the active surface area (S_{Cu}) was obtained by CO chemisorption on the same instrument. XPS spectra were

carried out on ESCALABMKLL X-ray photoelectron using an Al Kα source. Ultraviolet and visible (UV-Vis) absorption spectra were recorded by UV-vis spectrophotometer (Hitachi, U-3310) in the wavelength range of 400-800 nm.

3. Results and discussion

Nanostructures CuO with diverse morphologies have been prepared via a facile and scaleable wet-chemical method. Powder X-ray diffraction (XRD) was performed on the as-synthesized mesoporous CuO NPs with flower-, nanosheets-, bundle-, and dandelion-like shapes (Fig. S1). No other diffraction peak except CuO diffraction peaks can be detected, indicating that the as-prepared mesoporous CuO are high purity. The morphologies of the CuO NPs with flower-, nanosheets-, bundle-, and dandelion-like shapes were confirmed by SEM characterization (Fig. S2). The nitrogen physisorptions were investigated for the as-synthesized mesoporous CuO nanostructures with different morphologies (Fig. S3 and Table S1).

The as-prepared mesoporous CuO with diverse shapes were then reduced to mesoporous Cu as the catalysts (Fig. S4). The obtained mesoporous Cu with flower-, nanosheets-, bundle-, and dandelion-like shapes before the methanolysis of AB were characterized by powder XRD, SEM, TEM, HRTEM, XPS, N_2 adsorption-desorption and CO-TPD. As shown in Fig. 1, the diffraction peaks (2θ) of around 2θ = 43.34°, 50.47°, and 74.17° are ascribed to the (111), (200), and (220) planes of Cu, respectively, which can be indexed undisputedly to cubic Cu (JCPDS No. 04-0836). These results show that CuO nanostructures have been reduced to Cu nanostructures.

While a weak peak at around 36.45° is attributed to the partly surface oxidation of Cu during the process of sample preparation, which could not be avoided.[46,47]

SEM measurements were performed on all the nanostructured mesoporous Cu with diverse morphologies (flower-like, nanosheets-like, bundle-like and dandelion-like Cu) before the methanolysis of AB (Fig. 2). Fig. 2a indicates that the morphology of the Cu is flower-like, with a diameter about 5 μm and the nanobranches with average widths of 5 to 10 nm. As shown in Fig. 2b, the size of nanosheets-like Cu is 60 nm in thickness and 600 nm in length. The width and length of the bundle-like Cu particles are about 100~300 nm and 0.4~1 μm, respectively (Fig. 2c). The diameter of dandelion-like Cu is about 3~5 μm, and self-assembly of nanoplates with an average thickness of about 10-20 nm (Fig. 2d). Compared to the as-synthesized mesoporous CuO (Fig. S2), the morphologies of mesoporous Cu nanostructures have no significant changes after reduction reaction. Fig. 3a presents transmission electron microscopy (TEM) images of the flower-like Cu nanostructures before catalytic reaction. Meanwhile, a typical higher magnification TEM image of the terminal part of the individual flower-like Cu is shown in Fig. 3b. Fig. 3c depicts the HRTEM image of the region marked in Fig. 3b. As shown in Fig. 3c, it can be observed that the terminal part of the individual flower-like Cu with the clear lattice fringes, as an indicative of the high crystallinity of the nanostructure skeleton. The interplanar distance of 2.088 Å, 1.807 Å and 1.208 Å can be attributed to the cubic of Cu (111), (220) and (200) plane (JCPDS: 0836), respectively.

The XPS peaks for Cu 2p peaks were observed at 934.0 and 953.8 eV with strong

shaken-up satellite peaks at the as-synthesized flower-like CuO (Fig. S5). The strong satellite peaks confirm that the copper species of the as-synthesized sample is Cu(II). While after reduction with AB, the satellite peaks characteristic of Cu(II) species are disappeared. Similar feature is also observed in other mesoprorous CuO samples. This feature in the spectrum appearance is further assured that CuO were reduced to Cu by AB in the methanolysis reaction.

A nitrogen adsorption-desorption measurement shows that the flower-like, nanosheets-like, bundle-like, and dandelion-like Cu nanostructures before methanolysis of AB have a Brunauer-Emmett-Teller (BET) surface area of 7.39, 9.44 6.20, 7.28 m^2 g^{-1} (Table S2), respectively. The pore diameter and pore volume of mesoporous Cu are also listed in Table S2. Compared to those of the as-synthesized CuO (Table S1), the BET surface area, pore diameter, and pore volume of mesoporous Cu show a decrease after reduction reaction, which is due to that CuO has been reduced to Cu by AB during the methanolysis reaction. The typical IV isotherms with a hysteresis loop occur at a relative pressure of 0.8-1.0 (Fig. 4), showing the existence of mesopores in all the Cu nanostructures, which is further confirmed by the pore diameters (12.1~14.8 nm) of the samples (Table S2). The reactive surface of the mesoporous Cu nanostructures before the methanolysis of AB were performed on CO temperature programmed desorption (CO-TPD) titration measurements. As shown in the Table S3, the reactive surface of Cu are in the order of flower- > nanosheets- > bundle- > dandelion-like shape. The flower-like Cu shows the highest reactive surface area among those of the mesopores nanomaterials, in line with catalytic activity test

for the methanolyis of AB (vide infra).

Figure 5 shows the time course of the hydrogen generation from the methanolysis of AB (0.2 M, 5 mL) in the presence of the mesoporous Cu with different shapes. The results demonstrated that the reaction rate and the amount of hydrogen evolution significantly depended on their morphologies. As shown in Fig. 5, a stoichiometric amount of hydrogen (70 mL) is evolved in 8.3, 10.6, 13.3, 16.8 min, respectively, in the presence of the flower-like, nanosheets-like, bundle-like and dandelion-like Cu nanostructured catalysts. Clearly, among them the flower-like Cu exhibits the highest performance for the dehydrogenation of ammonia borane at room temperature for chemical hydrogen storage. Moreover, the turnover frequency (TOF) for this reaction in presence of flower-like, nanosheets-like, bundle-like and dandelion-like Cu nanostructured are measured to be 2.41, 1.89, 1.50, 1.19 mol H_2 mol catalyst^{-1} min^{-1}, respectively. The TOF value of the obtained flower-like Cu is higher than most of the Cu nanocatalysts ever reported for hydrogen generation from the solvolysis of AB (Table S4).[27,43-47] A rapid hydrogen generation starts immediately and then shows down continuously in Fig. 5, indicating that the TOF (activity) of the catalyst decreases with decreasing the NH_3BH_3 concentration as the reaction proceeds. Similar features were also observed in the previous reports (Ref. 22 & 27, etc.). Xu and coworkers point out that AB can interact with the surface of the metal particles to form an activated complex which dissociated upon attack of a water molecule to generate hydrogen.[45] A plausible mechanism of H_2 release in our case is shown in Fig. S6. As shown in the scheme, the release of H_2 is attributed to the attack of methanol

on a transient M-H. The formation of the transient could be the prerequisite for the methanolysis reaction.

To further study the catalytic activity of flower Cu for hydrogen generation from the methanolysis of AB, a series of experiments with different catalyst contents were performed, while the initial AB (0.2 M, 5 mL) concentration was kept unchanged. Fig. 6 shows the volume of hydrogen generated versus time during the catalytic methanolysis of AB (0.2 M, 5 mL) solution in the presence of flower-like Cu with different concentrations (0.022, 0.030, 0.037, 0.045 M) at room temperature. When the catalysts content increased, the reaction time decreased obviously from 10.4 min to 5.1 min. The hydrogen generation rate is determined from the linear portion of the plot for each reaction. The plot of hydrogen generation rate vs. Cu concentration in logarithmic scale is shown in the inset of Fig. 6. The slope of the line is calculated to be 0.93, which is closed 1, indicating that the methanolysis of AB by the catalyst of flower-like Cu is first-order with respect to the catalyst concentration. This is similar to the previous reports.[35,36,38,40]

Figure 7 shows the volume of hydrogen generated versus reaction time in the methanolysis of AB (0.2, 5 mL) catalyzed by flower-like Cu catalysts at various temperatures in the range of 293-308 K. Obviously, the rate of the reaction is enhanced by increasing the temperature. The reaction rate constant k at different temperatures has been estimated from the slope of the linear part of each plot in Fig. 7. The Arrhenius plot of lnk versus 1/T for the catalyst is plotted in Fig. 7 (inset), from which the activation energy (E_a) for the hydrogen release from the methanolysis of

AB is measured to be 34.2 ± 1.2 kJ mol^{-1}, which is lower than most of the reported activation energy values for the methanolysis and hydrolysis of AB using many different catalysts even with some noble-metal containing catalysts (Table S5), indicating the superior catalytic performance of flower-like Cu. The activation energy of nanosheets-like, bundle-like and dandelion-like Cu for dehydrogenation from AB in methanolysis are measured to be 35.0 ± 1.4, 38.5 ± 0.2, and 43.9 ± 0.5 kJ mol^{-1}, respectively (Figs. S7-S9).

The recyclability of flower-like Cu was tested at room temperature. After complete methanolysis of AB, the catalysts were kept in the reaction solution under ambient conditions, and a new AB (34.3 mg) was added to the reaction system 20 min later (Fig. S10). Fig. 8 shows the H_2 productivity and the activity percentage of the flower-like Cu retained in subsequent AB methanolysis. The catalyst retains 93% of its initial catalytic activity after the fifth run methanolysis of AB with 100% H_2 productivity (Fig. 8 & Fig. S11), due to that the regenerated Cu NPs maintain their high activity in the conversion between Cu^0 and Cu^{2+} cations (see ESI, Page S18 and S19). The observed slight decrease in catalytic activity in successive runs is likely caused by the increase in solution viscosity during the AB methanolysis. After recycle test, the catalyst was separated from the reaction solution and characterized by SEM. As shown in the Fig. S12, the shape of the 5^{th} flower-like Cu was transferred to irregular shape Cu NPs, probably due to the conversion between Cu^0 and Cu^{2+} cations after many cycles.

4. Conclusions

In summary, we have successfully synthesized flower-like, nanosheets-like, bundle-like and dandelion-like CuO nanostructures by a simple wet-chemical method. The as-synthesized mesoporous CuO nanostructures were firstly reduced to mesoporous Cu nanostructures and used as a robust cost-effective catalyst for hydrogen generation from the methanolysis of AB at room temperature. Among the four Cu nanostructures, the flower-like Cu exhibits the highest catalytic activity with the total turnover frequency (TOF) of 2.41 mol H_2 mol catalyst^{-1} min^{-1} for hydrogen generation from the methanolysis of AB. Moreover, the activation energy for the flower-like Cu is measured to be about 34.2 ± 1.2 kJ mol^{-1}, which is lower than most of the reported activation energy values for the methanolysis and hydrolysis of AB using many different catalysts even for some noble-metal containing catalysts, indicative of the superior catalytic performance of flower-like Cu nanostructure. The flower-like Cu nanostructures also exhibit an excellent activity in the recyclability experiments. The high catalytic activity and low cost of the shape-controlled mesoporous Cu nanostructures display promising in replacing noble-based metal catalysts for the practical application in hydrogen generation from the methanolysis of AB.

Acknowledgement

This work was financially supported by National Natural Science Foundation of China (No. 21103074 and No. 21463012), Jiangxi Provincial Education Department

(No. GJJ14230), Natural Science Foundation of Jiangxi Province of China (No. 20114BAB203010 and No. 20132BAB203014). Z.-H. Lu was supported by the Sponsored Program for Cultivating Youths of Outstanding Ability in Jiangxi Normal University, Young Scientist Foundation of Jiangxi Province (20133BCB23011), and "Gan-po talent 555" Project of Jiangxi Province.

References

1. N. L. Rosi, J. Eckert, M. Eddaoudi, D. T. Vodak, J. Kim, M. O'Keeffe and O. M. Yaghi, *Science*, 2003, **300**, 1127.
2. X. Gu, Z. H. Lu, Q. Xu, H. L Jiang, T. Akita and Q. Xu, *J. Am. Chem. Soc*., 2011, **133**, 11822.
3. U. B. Demirci and P. Miele, *Energy Environ. Sci*., 2011, **4**, 3334.
4. G. A. Deluga, J. R. Salge, L. D. Schmidt and X. E. Verykios, *Science*, 2004, **303**, 993.
5. L. Schlapbach and A.Zuttel, *Nature*, 2001, **414**, 353.
6. P. Chen, Z. T. Xiong, J. Z. Luo, J. Y. Lin and K. L. Tan, *Nature*, 2002, **420**, 302.
7. Z. H. Lu and Q. Xu, *Funct. Mater. Lett*., 2012, **5**, 1230001.
8. Z. H. Lu, Q. L. Yao, Z. J. Zhang, Y. W. Yang and X. S. Chen, *J. Nanomater*., 2014, 729029.
9. B. Peng and J. Chen, *Energy Environ. Sci*., 2008, **1**, 479.
10. U. B. Demirci and P. Miele, *Energy Environ. Sci*., 2009, **2**, 627.
11. M. Yadav and Q. Xu, *Energy Environ. Sci*., 2012, **5**, 9698.

12. H. L. Jiang and Q. Xu, *Catal. Today*, 2011, **170**, 56.

13. C. W. Hamilton, R. T. Baker, A. Staubitz and I. Manners, *Chem. Soc. Rev*., 2009, **38**, 279.

14. F. H. Stephens, V. Pons and R. T. Baker, *Dalton Trans*., 2007, 2613.

15. N. Mohajeri, A. T. Raissi and O. Adebiyi, *J. Power Sources*, 2007, **167**, 482.

16. P. V. Ramachandran and P. D. Gagare, *Inorg. Chem*., 2007, **46**, 7810.

17. W. Grochala and P. P. Edwards, *Chem. Rev*., 2004, **104**, 1283.

18. M. Ramzan, F. Silvearv, A. Blomqvist, R. H. Scheicher, S. Lebegue and R. Ahuja, *Phys. Rev. B*, 2009, **79**, 132102.

19. Z. H. Lu, H. L. Jiang, M. Yadav, K. Aranishi and Q. Xu, *J. Mater. Chem*., 2012, **22**, 5065.

20. J. M. Yan, X. B. Zhang, S. Han, H. Shioyama and Q. Xu, *Inorg. Chem*., 2009, **48**, 7389.

21. Z. H. Lu, J. P. Li, A. L. Zhu, Q. L. Yao, W. Huang, R. Y. Zhou, R. F. Zhou and X. S. Chen, *Int. J. Hydrogen Energy*, 2013, **38**, 5330.

22. M. Chandra and Q. Xu, *J. Power Sources*, 2006, **156**, 190.

23. S. Akbayrak and S. Özkar, *Dalton Trans*., 2014, **43**, 1797.

24. Ö. Metin, V. Mazumder, S. Özkar and S. H. Sun, *J. Am. Chem. Soc*., 2010, **132**, 1468.

25. Q. L. Zhu, J. Li and Q. Xu, *J. Am. Chem. Soc*., 2013, **135**, 10210.

26. Q. L. Yao, W. M. Shi, G. Feng, Z. H. Lu, X. L. Zhang, D. J. Tao, D. J. Kong, and X. S. Chen, *J. Power Sources*, 2014, **257**, 293.

27. Y. W. Yang, Z. H. Lu, Y. J. Hu, Z. J. Zhang, W. M. Shi, X. S. Chen and T. T. Wang, *RSC Advances*, 2014, **4**, 13749.

28. Z. H. Lu, J. P. Li, G. Feng, Q. L. Yao, F. Zhang, R. Zhou, D. Tao, X. Chen and Z. Q. Yu, *Int. J. Hydrogen Energy*, 2014, **39**, 13389.

29. Q. L. Yao, X. S. Chen and Z. H. Lu, *Energy Environ. Focus*, 2014, **3**, 236.

30. Y. Yamada, K. Yano and S. Fukuzumi. *Energy Environ. Sci*., 2012, **5**, 5356.

31. M. Kaya, M. Zahmakiran, S. Özkar and M. Volkan, *ACS Appl. Mater. Interfaces*, 2012, **4**, 3866.

32. Y. Yamada, K. Yano, Q. Xu and S. Fukuzumi, *J. Phys. Chem. C*, 2010, **114**, 16456.

33. J. M. Yan, Z. L. Wang, H. L. Wang and Q. Jiang, *J. Mater. Chem*., 2012, **22**, 10990.

34. Y. S. Du, N. Cao, L. Yang, W. Luo and G. Z. Cheng, *New J. Chem*., 2013, **37**, 3035.

35. H. Erdogan, Ö. Metin and S. Özkar, *Phys. Chem. Chem. Phys*., 2009, **11**, 10519.

36. H. Erdogan, Ö. Metin and S. Özkar, *Catalysis Today*, 2011, **170**, 93.

37. S. Çalışkan, M. Zahmakıran and S. Özkar, *Appl. Catal. B-Environ*., 2010, **93**, 387.

38. H. B. Dai, X. D. Kang and P. Wang, *Int. J. Hydrogen Energy*, 2010, **35**, 10317.

39. D. H. Sun, V. Mazumder, Ö Metin and S. H. Sun, *ACS Catal*., 2012, **2**, 1290.

40. S. B. Kalidindi, A. A. Vernekar and B. R. Jagirdar, *Phys. Chem. Chem. Phys*., 2009, **11**, 770.

41. Y. X. Zhang, M. Huang, F. Li and Q. W. Zhong, *Int. J. Electrochem. Sci*., 2013, **8**, 8645.

42. Y. X. Zhang, M. Kuang, M. Huang and Q. W. Zhong, I*nt. J. Electrochem. Sci*., 2013, **8**, 9723.

43. M. Zahmakiran, F. Durap and S. Özkar, *Int J. Hydrogen Energy*, 2010, **35**, 187.

44. O. Ozay, E. Inger, N. Aktas and N. Sahiner, *Int. J. Hydrogen Energy*, 2011, **36**, 8209.

45. Q. Xu and M. Chandra, *J. Power Sources*, 2006, **163**, 364.

46. S. B. Kalidindi, M. Indirani and B. R. Jagirda, *Inorg. Chem*., 2008, **47**, 7424.

47. S. B. Kalidindi, U. Sanyal and B. R. Jagirdar, *Phys. Chem. Chem. Phys*., 2008, **10**, 5870.

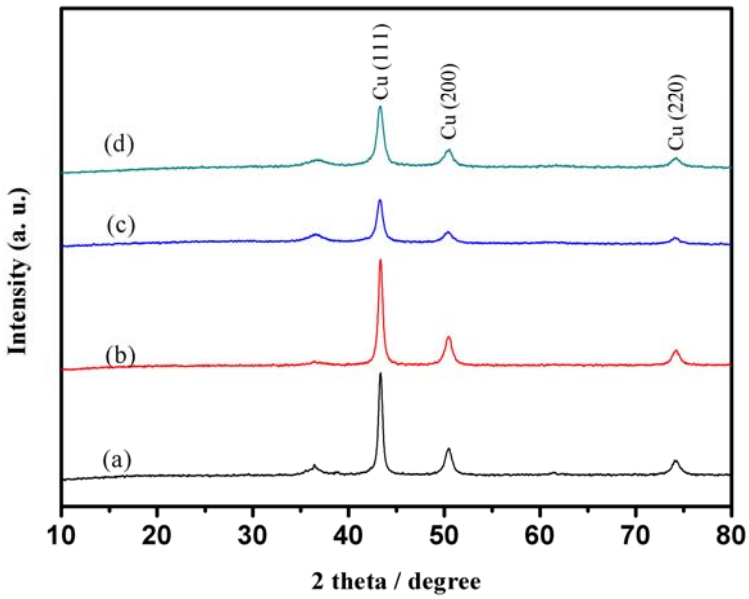

Fig. 1 Powder X-ray diffraction patterns of the mesoporous Cu nanostructures with a) flower-like, b) nanosheets-like, c) bundle-like, and d) dandelion-like shape before the methanolysis of NH_3BH_3.

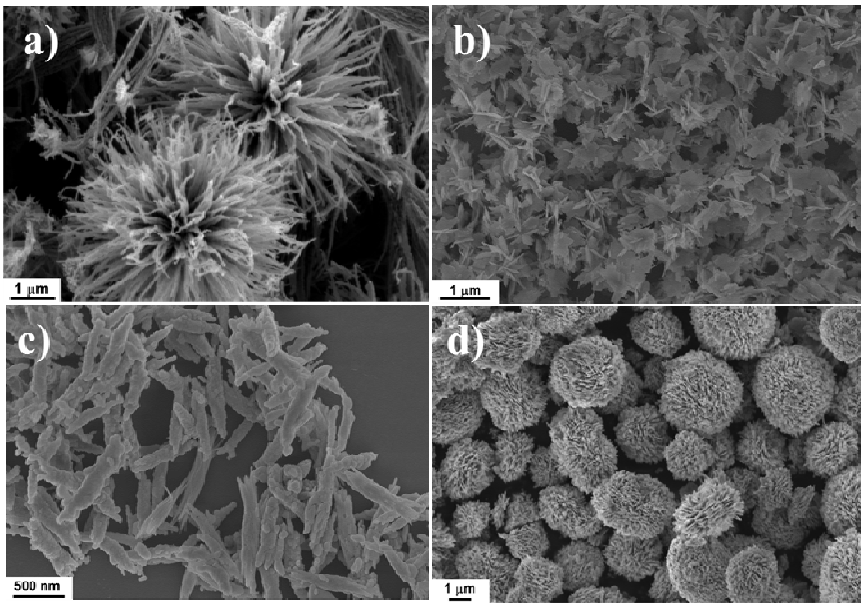

Fig. 2 SEM images of the mesoporous Cu nanostructures with a) flower-like, b) nanosheets-like, c) bundle-like, and d) dandelion-like shape before the methanolysis of NH_3BH_3.

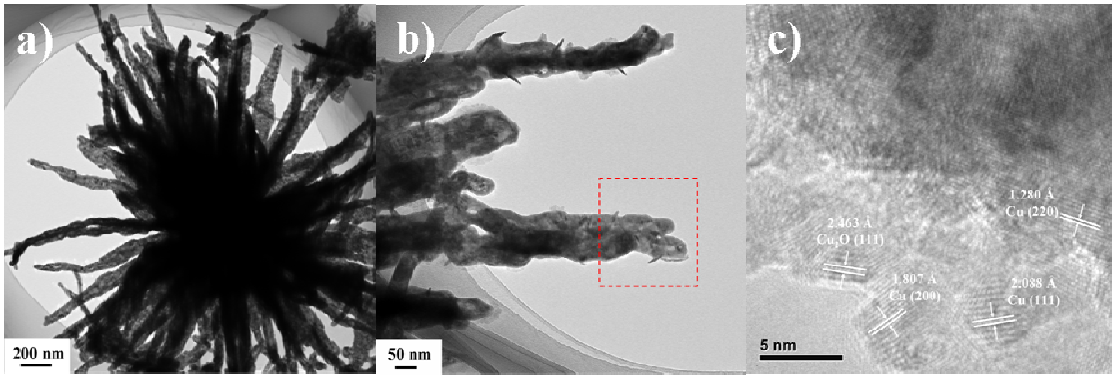

Fig. 3 a,b) TEM images and c) HRTEM image (the region marked in b) of the flower-like Cu before the methanolysis of NH_3BH_3.

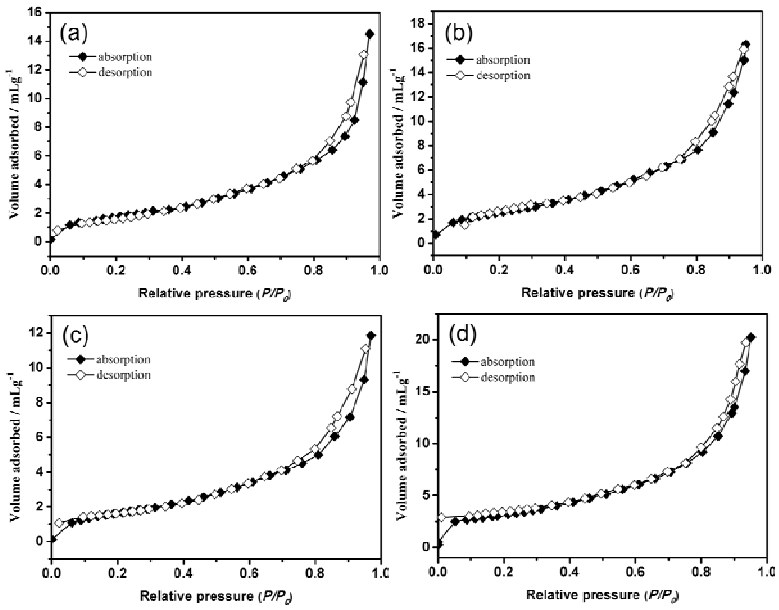

Fig. 4 Nitrogen adsorption-desorption isotherms of the mesoporous Cu nanostructures with a) flower-like, b) nanosheets-like, c) bundle-like, and d) dandelion-like shape before the methanolysis of NH_3BH_3.

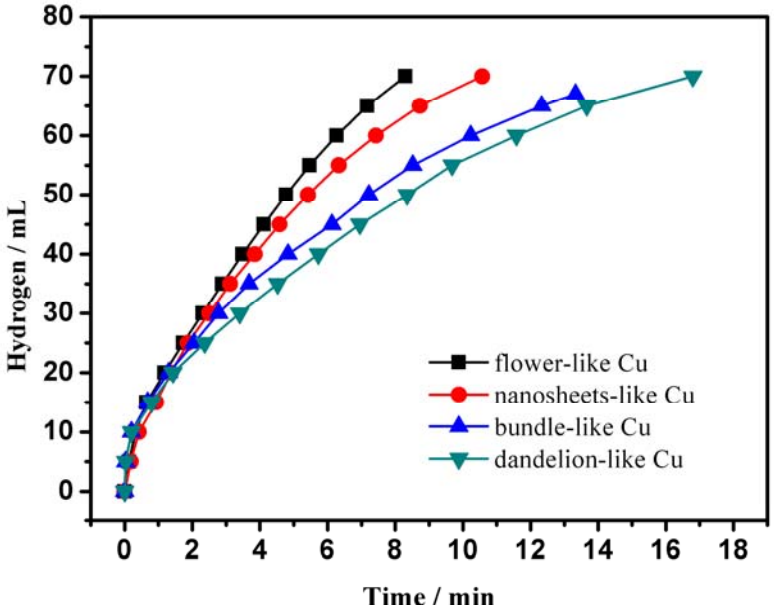

Fig. 5 Hydrogen generation from the methanolysis of NH_3BH_3 (0.2 M, 5 mL) in the presence of mesoporous Cu with diverse morphologies at 298 K ($Cu/NH_3BH_3 = 0.15$).

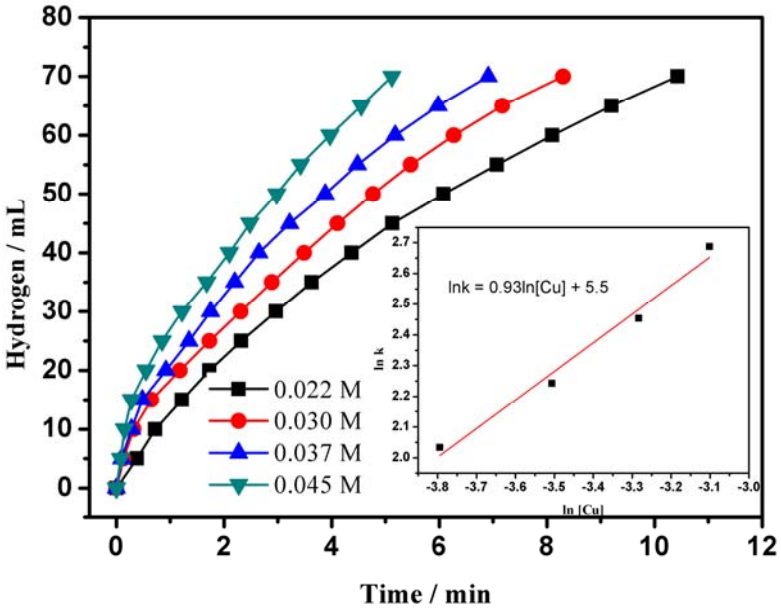

Fig. 6 Hydrogen generation from the methanolysis of NH_3BH_3 (0.2 M, 5 mL) in the presence of flower-like Cu with different catalyst concentrations at 298 K. The inset shows the plot of hydrogen generation rate vs. the concentration of Cu, both in logarithmic scale.

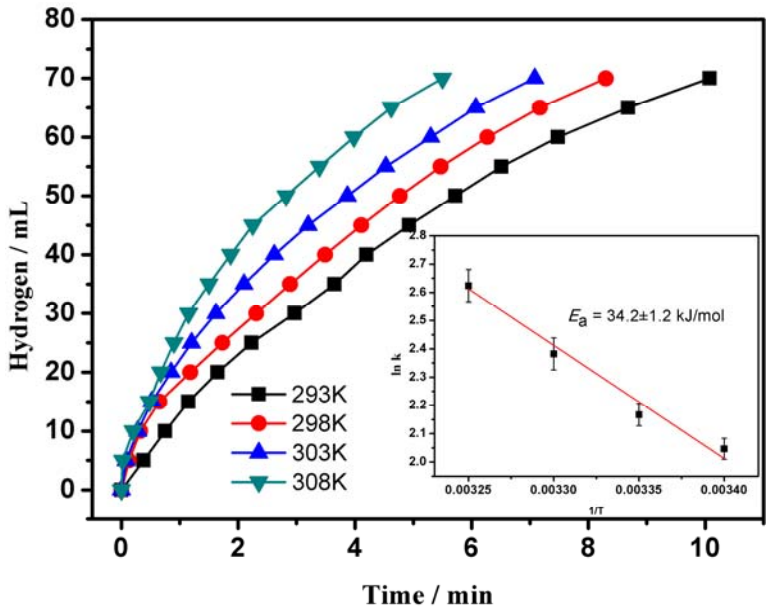

Fig. 7 Hydrogen generation from the methanolysis of NH_3BH_3 (0.2 M, 5 mL) in the presence of flower-like Cu at 293-308 K (Cu/NH_3BH_3 = 0.15). The inset shows the Arrhenius plot (ln k vs. 1/T).

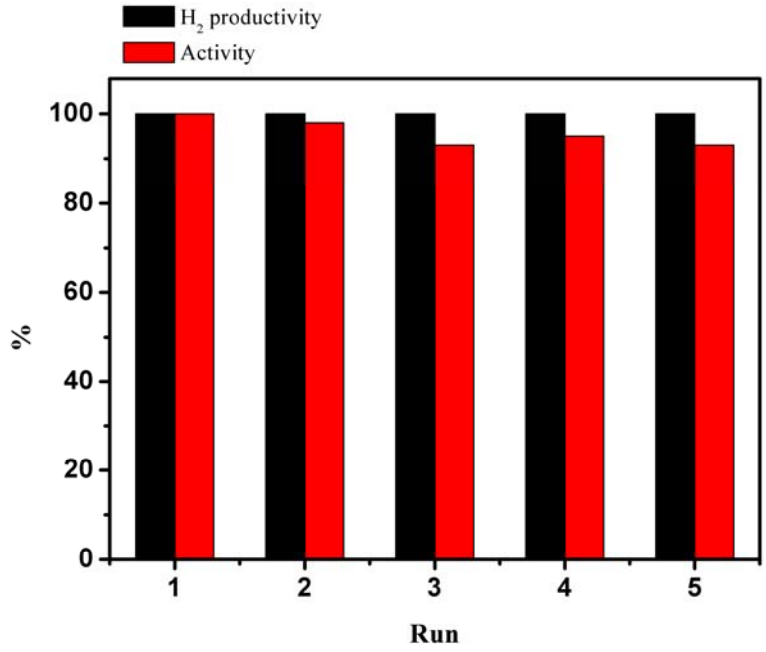

Fig. 8 Percentage of initial catalytic activity of the flower-like Cu at sequential catalytic runs for the methanolysis of NH_3BH_3 at 298 K ($Cu/NH_3BH_3 = 0.15$).